Broadband, slow sound on a glide-symmetric meander-channel surface

J. G. Beadle,[a] I. R. Hooper, J. R. Sambles, and A. P. Hibbins
Electromagnetic and Acoustic Materials Group, Department of Physics and Astronomy, Physics Building, Stocker Road, University of Exeter, Exeter, EX4 4QL, United Kingdom

(Received 1 February 2019; revised 25 April 2019; accepted 9 May 2019; published online 31 May 2019)

The acoustic surface waves supported by hard surfaces patterned with repeat-period, meandering grooves are explored. The single, continuous groove forms a glide-symmetric surface, inhibiting the formation of a bandgap at the first Brillouin-zone boundary. Consequently, the acoustic surface waves exhibit an almost constant, sub-speed-of-sound, group velocity over a broad frequency band. Such slow, broadband modes may have applications in controlling the flow of noise over surfaces.
 https://doi.org/10.1121/1.5109549

[BA] Pages: 3190–3194

I. INTRODUCTION

The patterning of surfaces to control sound propagation has been the topic of many studies with increasing interest over recent years. This includes structuring surfaces to manipulate acoustic surface waves (ASWs) (Kelders *et al.*, 1998a; Kelders *et al.*, 1998b; Tizianel *et al.*, 1998) leading to, for example, increased acoustic transmission (Christensen *et al.*, 2007), or scattering from arrays of elastic scatterers to create sonic crystals that attenuate transmission (García-Chocano *et al.*, 2012; Martínez-Sala *et al.*, 1995; Sánchez-Pérez *et al.*, 1998). A number of works have shown that it is possible to control the propagation of sound waves using arrays of subwavelength elements (phononic crystals) as first proposed by Kock and Harvey (Kock, 1949), or more recently the study of labyrinthine structures (Frenzel *et al.*, 2013; Xie *et al.*, 2013) Recently Liang and Li (2012) demonstrated that, by using curled perforations to coil up space, large effective refractive indices (n) can be achieved. This allows the potential to spatially engineer n and create arrays of such structures of various different acoustic path lengths to control phase-gradients allowing for the focusing, absorption, and directing of acoustic waves, as well as "doubly negative" material properties and an effective "density" near zero. Other structured surfaces have been used to control waves, such as a subwavelength corrugated surface demonstrated by Zhu *et al.* (2015) where, by manipulating the dispersionless phase fronts, ultra-broadband extraordinary reflection could be obtained. Fan *et al.* (2018) found that by enclosing a monopole sound source in a structure comprised of various space-coiled element allows for the device to be 1/10 the size of the wavelength emitted.

While being able to reduce the velocity of propagation of acoustic energy over a surface is itself interesting and undoubtedly useful, for some applications one may require this to be maintained over a broad frequency band. In general, this is difficult to achieve with a periodically patterned or resonant surface because of diffraction and mode-hybridisation, the former being particularly dominant on approach to the first Brillouin zone boundary. Glide symmetric structures (Crepeau and McIsaac, 1964; Hessel *et al.*, 1973) offer an opportunity to maintain low-group-velocity ASWs, as has been demonstrated in electromagnetism (Mitchell-Thomas *et al.*, 2017). They are comprised of a geometry that has reflection symmetry about a mirror plane when the unit cell is displaced by half a period. In this way, these structures do not present a bandgap due to two degenerate energy states existing at the first Brillouin-zone boundary(Camacho *et al.*, 2017; Quesada, 2014), resulting in a near-linear dispersion across a broad bandwidth.

Here, ASWs propagating over various finite-depth periodic meandering channels that have glide symmetry in acoustically-rigid materials are investigated.

II. THEORY

The dispersion of the bound surface modes has been characterised by measuring their propagation across the surface via near-field excitation and detection. To the authors' knowledge this is the first time that ASWs above such space-coiled structures have been measured and characterised.

A meander channel of depth d, and width w, as illustrated in Fig. 1(a) is explored. The channel is space-coiled in a glide-symmetric unit cell with repeat period of λ_g along the direction of propagation. By taking a simple geometrical approach, a wave following the channel across one unit cell will propagate along a path-length of

$$l_p = 2(\pi r + h), \tag{1}$$

where r is the radius of the curved channel sections and h is the length of the straight sections of the channels. This increase in path length in relation to the unit cell can be thought of as creating an effective waveguide index, given by

$$n_{wg} = \frac{l_p}{\lambda_g}, \tag{2}$$

if the power propagation is confined to the grooves, then this is directly related to the group index. A simple dispersion

[a]Electronic mail: jgb206@exeter.ac.uk

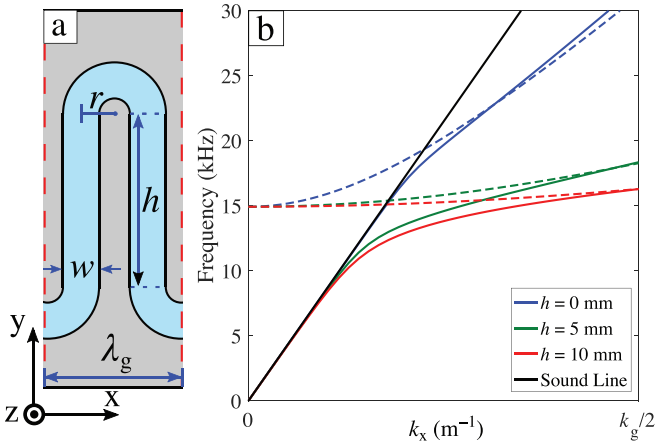

FIG. 1. (a) Schematic of the surface of a unit cell used in this investigation, comprised of an air-filled channel (blue line) of depth $d = 5$ mm in an acoustically-rigid material (gray line). The depth is in the negative z direction, and the ASW propagates in the positive x-direction. Here, $\lambda_g = 4$ mm, $w = r = 1$ mm, and $h = 5$ mm. (b) Waveguide approximation from Eq. (3) (non-solid, coloured lines) and finite element model (solid lines) dispersion for different values of h. The solid black line corresponds to the maximum wavevector of an incident plane wave. Modes beyond this limit are trapped at the surface (ASWs) since they are unable to couple into plane waves.

relation for such a structure can be established since, to first order, the wavevector in the vertical direction (depth of grooves) is given by the quarter wavelength resonator condition $k_z = 2\pi/4d$ [ignoring end effect corrections (Kinsler *et al.*, 1999)]. With the wavevector in the propagation direction given by k_x it follows that the dispersion relation is simply

$$f = \frac{v}{2\pi}\sqrt{\left(\frac{k_x}{n_{wg}}\right)^2 + \left(\frac{2\pi}{4d}\right)^2}. \tag{3}$$

The effect of varying h on the dispersion is considerable, as seen in Fig. 1(b). Here, we show the approximate analytic dispersion from Eq. (3), together with the predictions of finite element method (FEM) modeling using Comsol Multiphysics (COMSOL AB). Since the simple analytic model neglects any interactions with free-space sound modes and diffractive coupling between adjacent grooves there is a significant disagreement between the two models at wavevectors within and close to the sound line. However, at values of $k_x > k_0$ [where $k_0^2 = (2\pi f/c)^2 = k_x^2 + k_z^2$], the mode becomes more confined to the surface and therefore the channel, and hence Eq. (3) provides a good approximation. Of course, Eq. (3) does not include any diffraction effects, but it is clear from the FEM model that the modes have a linear dispersion (and uniform group velocity) approaching the first Brillouin zone boundary ($k_g/2$)—a consequence of the glide symmetry of the system (Hessel *et al.*, 1973).

III. METHOD

To experimentally determine the dispersion of the ASWs, a loudspeaker with a sound-launching conical attachment was positioned so that the sound emitted was angled onto the surface (Fig. 2). The narrow exit hole of the cone and close proximity to the surface leads to strong diffraction and enables near-field coupling to the ASW. One of the main difficulties with obtaining results was to the signal from the surface mode being dominated by free radiation. To achieve this, the needle microphone (Brüel & Kjær Probe Microphone type 4182, Brüel & Kjær, Nærum, Denmark) with its tip about 0.5 mm from the surface was then raster-scanned over the sample to detect the near-fields with a resolution of 1 mm and a total scan length (x) of 300 mm. The signature of free radiation appears on the dispersion along the sound line ($k_x = k_0$). This signal eventually dominates at high k_x when the surface modes become progressively more confined and their intensity is very low. At each microphone position, a 30 kHz near-single-cycle Gaussian-envelope (broadband) sound pulse was emitted from the loudspeaker and subsequently detected by the microphone. For each spatial position an average of three pulses was taken to improve the signal to noise. Subsequently a temporal Fourier transform was performed to obtain the amplitude and phase for each frequency at each spatial position, resulting in a spatial field-map for each frequency. A two-dimensional Fast Fourier Transform (FFT) was then performed on each of the spatial field maps. By plotting the Fourier amplitudes as a function of wavevector from each of these two-dimensional FFTs for each frequency one obtains a representation of dispersion diagram of the ASWs supported (Beadle *et al.*, 2018). As the group velocity ($v_g = \mathrm{d}\omega/\mathrm{dk}$, where ω is the angular frequency) is the gradient of the mode, it was calculated by fitting a straight line to the near-linear region of the surface mode.

Five aluminum samples have been characterized, each 600 mm in length (x): three samples comprised of 150 unit cells, each with $\lambda_g = 4$ mm, $w = 1$ mm, and straight line sections of $h = 0$ mm (i), 5 mm (ii), 10 mm (iii); a further sample (iv) (100 unit cells) has $\lambda_g = 6$ mm, $w = 2$ mm, and $h = 5$ mm. A fifth sample (v) is a modified version of (ii) with tape placed over part of the meander [as in Fig. 3(b)] to remove the glide symmetry.

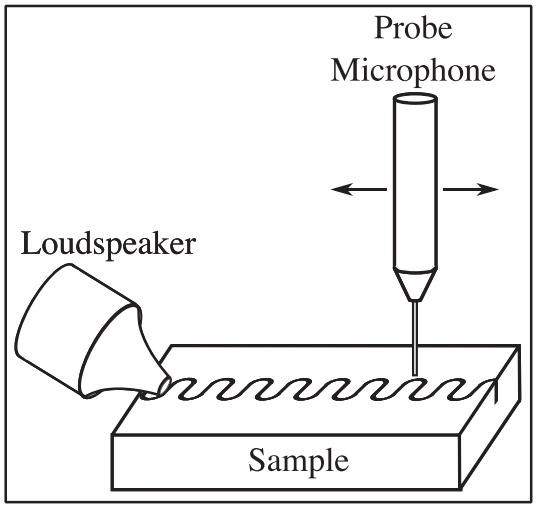

FIG. 2. Schematic of the experimental setup. A loudspeaker with conical attachment emits a broadband-pulse that excites the ASW. This then propagates over the surface and the arriving pulse is recorded using a near-field probe that is raster scanned over the surface.

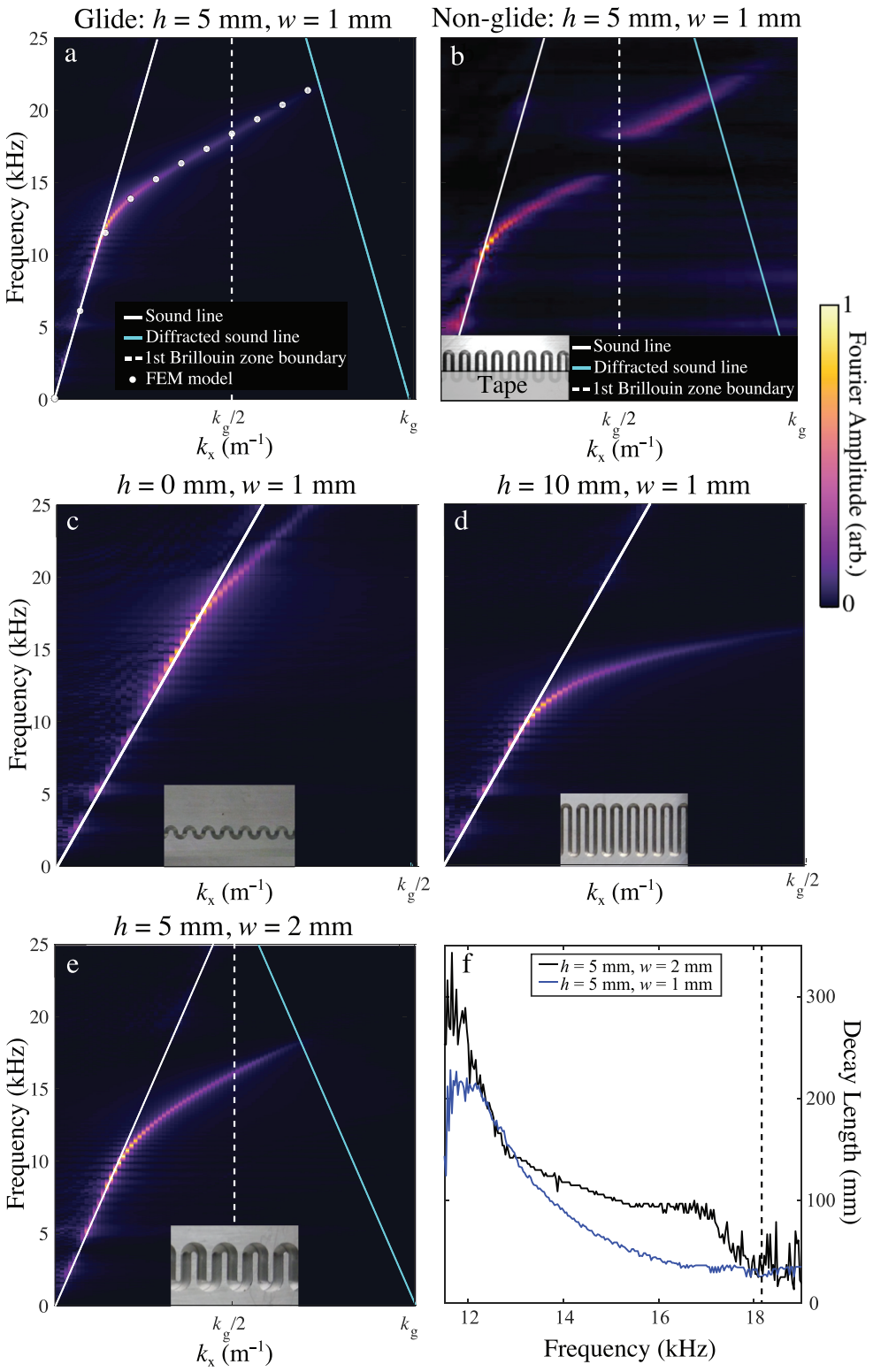

FIG. 3. (a)–(e) Two-dimensional FFT of the experimental field data recorded at a height of 0.5 mm across the surface, illustrating the dispersion of the surface mode supported by each of the investigated structures: (a) $h = 5$ mm, $w = 1$ mm, also shown are predictions from the FEM model (symbols), (b) $h = 5$ mm, $w = 1$ mm, but with the glide-symmetry broken. (c) $h = 0$ mm, $w = 1$ mm. (d) $h = 10$ mm, $w = 1$ mm. (e) $h = 5$ mm, $w = 2$ mm. Note the different x axis extent in (c) and (d). (f) Decay length as a function of frequency for the two different widths and $h = 5$ mm samples. The vertical dashed line indicates the diffraction edge ($k_x = k_g$ - k_0) for the $h = 5$ mm, $w = 2$ mm sample.

IV. DISCUSSION

Figure 3(a) shows a typical experimentally determined dispersion plot for the $\lambda_g = 4$ mm and $h = 5$ mm surface. Below 10 kHz the mode is essentially non-dispersive and propagates as a grazing mode at the speed of sound. From 10 to 14 kHz there is strong frequency dependence of both the phase and group velocity as the mode moves from being a lightly-bound surface wave to being more like a waveguide mode confined to the channel. Then, at higher frequencies

up to 21 kHz, the mode has a nearly constant gradient, corresponding to a constant group velocity, but a changing phase velocity (v_p). For this particular sample in the vicinity of 20 kHz the group velocity is $v_g = 55.6\ (\pm 4.1)\ \mathrm{ms}^{-1}$, a reduction by a factor of 6 below that of the speed of sound in air. Note that the FEM model predicts $v_g = 57.1\ \mathrm{ms}^{-1}$ which is in excellent agreement with the experimental data.

The frequency range for which a near constant group velocity is observed is extended in k_x due to the absence of a bandgap at the first Brillouin zone boundary in comparison to the non-glide case, a consequence of the glide symmetry of the structure. This glide symmetry condition may be readily broken by applying a tight membrane over part of the meander sample. This was done using parcel tape with the tape edge aligned parallel to the propagation direction with the tape covering $\sim$20% of the meander of the $h = 5$ mm sample, as seen in the inset of Fig. 3(b). The resulting ASW is now very different; no longer does the mode have a constant group velocity over a wide bandwidth, instead a large bandgap has opened between 16 and 18 kHz resulting in the mode becoming dispersive.

The effect of changing l_p on the dispersion of the ASW is seen in Figs. 3(c) and 3(d). Using the simple analytic Eq. (3) we predict that n_{wg} at high k_x has values of 1.57 and 8.14 for the $h = 0$ and 10 mm samples, respectively. For the $h = 0$ sample the analytical result compares favourably with those from the full modeling shown in Fig. 1(b) which give 1.76. For the 10 mm sample the full model value of 10.70 agrees less well since the analytic treatment neglects end effects as well as interactions with the free-space sound. For these two surfaces v_g has been measured and values of 192.4 ($\pm$15.1) ms^{-1} and 33.4 ($\pm$3.1) ms^{-1} were found, respectively, giving values for n_{wg} of 1.78 ($\pm$0.14) and 10.28 ($\pm$0.96). Both values are in close agreement with the Comsol model.

It is also of interest to explore the propagation length of the ASW in the x-direction over the meander surface. Attenuation will occur due to the thermal and viscous boundary layers within the structure. The thermal boundary layer arises from the isothermal boundary condition between the rigid wall and the air-filled cavity. Because of this a temperature gradient exists where heat is transferred into the wall of the cavity acting as a dissipative process. The viscous boundary layer exists due to a no-slip boundary layer between the solid and air-filled cavity. A gradient in the parallel component of the particle velocity now arises within the air, resulting in lost energy due to momentum transfer. One may describe the decay of the ASW as the distance over which the amplitude of the absolute pressure field decays to 1/e. This decay length was measured as a function of frequency. To further investigate the decay length, one sample (v) with a wider channel ($w = 2$ mm) was fabricated. The dispersion plot for the ASW on this sample is shown in Fig. 3(f) with the inset showing a section of the sample. Notice that the dispersion of the mode curves away from the sound line more slowly before becoming linear. This arises from diffractive coupling between adjacent grooves. Similar coupling has been described by Zhu *et al.* (2013) for the case of isolated cavities supporting zero-velocity (trapped) modes, however, the coupling in the presented structure becomes dominated by the direct propagation along the groove as the mode becomes more strongly confined at higher frequency. This results in the dispersion curve for the channel with the largest h having the least linear region. Figure 3(f) shows the decay lengths as a function of frequency for the two different width $h = 5$ mm samples. As the channel width decreases, the attenuation of the surface waves increases; this is expected as the thermal and viscous boundary layers now occupy a larger proportion of the channel. In addition, the decay of the ASW for the $w = 2$ mm sample shows a second, steeper, decay beyond 17 kHz. At these frequencies the fields are becoming more strongly localised in the curved ends of the channels. With the fields in the transverse direction falling to zero over a distance of about 5 mm (the channel length in the transverse direction) then the characteristic wave dimension in the transverse direction is of order 20 mm. Thus these localised strong fields may now give rise to free radiation of this wavelength. This extra loss channel appears to come in at about 17 kHz. Up until that frequency once the dispersion has deviated from the sound line the decay length in the wider channel is more than twice that in the narrower channel.

V. CONCLUSIONS

In this study, glide-symmetric metasurfaces composed of space-coiled (meandering) cavities have been studied and show a broadband reduction in the group velocity of the supported ASWs. We have shown that as the length of the meander is increased, the group velocity decreases, with values of 192.4 ($\pm$15.1) ms^{-1}, 55.6 ($\pm$4.1) ms^{-1}, and 33.4 ($\pm$3.1) ms^{-1} obtained for different length channels. An increase in the channel width also results in a decreased attenuation of the ASWs due to the thermoviscous boundary layers occupying a smaller proportion of the channel. This work may lead to a novel structure for controlling the propagation of acoustic power over such surfaces.

ACKNOWLEDGMENTS

The authors wish to acknowledge financial support from the Engineering and Physical Sciences Research Council (EPSRC) of the United Kingdom, via the EPSRC Centre for Doctoral Training in Metamaterials (Grant No. EP/L015331/1) and QinetiQ. I.R.H. also acknowledges support from the EPSRC and QinetiQ Ltd. via the TEAM-A prosperity partnership (Grant No. EP/R004781/1). All data created during this research are openly available from the University of Exeter's institutional repository at https://ore.exeter.ac.uk/.

Beadle, J. G., Starkey, T., Dockrey, J. A., Sambles, J. R., and Hibbins, A. P. (**2018**). "The acoustic phase resonances and surface waves supported by a compound rigid grating," Sci. Rep. **8**, 10701.

Camacho, M., Mitchell-Thomas, R. C., Hibbins, A. P., Sambles, J. R., and Quevedo-Teruel, O. (**2017**). "Designer surface plasmon dispersion on a one-dimensional periodic slot metasurface with glide symmetry," Opt. Lett. **42**, 3375–3378.

Christensen, J., Fernandez-Dominguez, A. I., de Leon-Perez, F., Martin-Moreno, L., and Garcia-Vidal, F. J. (**2007**). "Collimation of sound assisted by acoustic surface waves," Nat. Phys. **3**, 851–852.

COMSOL AB. "COMSOL Multiphysics{®}," available at www.comsol.com (Last viewed May 21, 2019).

Crepeau, P. J., and McIsaac, P. R. (**1964**). "Consequences of symmetry in periodic structures," Proc. IEEE **52**, 33–43.
Fan, X. D., Zhu, Y. F., Liang, B., Cheng, J. C., and Zhang, L. (**2018**). "Converting a monopole emission into a dipole using a subwavelength structure," Phys. Rev. Appl. **9**, 034035.
Frenzel, T., Brehm, J. D., Bückmann, T., Schittny, R., Kadic, M., and Wegener, M. (**2013**). "Three-dimensional labyrinthine acoustic metamaterials," Appl. Phys. Lett. **103**, 061907.
García-Chocano, V. M., Cabrera, S., and Sánchez-Dehesa, J. (**2012**). "Broadband sound absorption by lattices of microperforated cylindrical shells," Appl. Phys. Lett. **101**(18), 184101.
Hessel, A., Oliner, A. A., Chen, M. H., and Li, R. C. M. (**1973**). "Propagation in periodically loaded waveguides with higher symmetries," Proc. IEEE **61**, 183–1953.
Kelders, L., Allard, J. F., and Lauriks, W. (**1998a**). "Ultrasonic surface waves above rectangular-groove gratings," J. Acoust. Soc. Am. **103**, 2730–2733.
Kelders, L., Lauriks, W., and Allard, J. F. (**1998b**). "Surface waves above thin porous layers saturated by air at ultrasonic frequencies," J. Acoust. Soc. Am. **104**, 882–889.
Kinsler, L. E., Frey, A. R., Coppens, A. B., and Sanders, J. V. (**1999**). *Fundamentals of Acoustics*, 4th ed. (Wiley, New York), Vol. 1, 274 pp.
Kock, W. E. (**1949**). "Refracting sound waves," J. Acoust. Soc. Am. **21**, 471–481.
Liang, Z., and Li, J. (**2012**). "Extreme acoustic metamaterial by coiling up space," Phys. Rev. Lett. **108**, 114301.
Martínez-Sala, R., Sancho, J., Sánchez, J. V., Gómez, V., Llinares, J., and Meseguer, F. (**1995**). "Sound attenuation by sculpture," Nature **378**, 241.
Mitchell-Thomas, R. C., Sambles, J. R., and Hibbins, A. P. (**2017**). "High index metasurfaces for graded lenses using glide symmetry," in *11th European Conference on Antennas Propagation (EUCAP)*.
Quesada, R. (**2014**). "Waveguiding enabled by coupled conformal surface plasmons," Opt. Lett. **39**, 2990–2993.
Sánchez-Pérez, J. V., Caballero, D., Mártinez-Sala, R., Rubio, C., Sánchez-Dehesa, J., Meseguer, F., Llinares, J., and Gálvez, F. (**1998**). "Sound attenuation by a two-dimensional array of rigid cylinders," Phys. Rev. Lett. **80**, 5325–5328.
Tizianel, J., Allard, J. F., and Brouard, B. (**1998**). "Surface waves above honeycombs," J. Acoust. Soc. Am. **104**, 2525–2528.
Xie, Y., Popa, B. I., Zigoneanu, L., and Cummer, S. A. (**2013**). "Measurement of a broadband negative index with space-coiling acoustic metamaterials," Phys. Rev. Lett. **110**, 175501.
Zhu, J., Chen, Y., Zhu, X., Garcia-Vidal, F. J., Yin, X., Zhang, W., and Zhang, X. (**2013**). "Acoustic rainbow trapping," Sci. Rep. **3**, 1–6.
Zhu, Y. F., Zou, X. Y., Li, R. Q., Jiang, X., Tu, J., Liang, B., and Cheng, J. C. (**2015**). "Dispersionless manipulation of reflected acoustic wavefront by subwavelength corrugated surface," Sci. Rep. **5**, 1–12.